Structural and magnetic characterization of batch-fabricated nickel encapsulated multi-walled carbon nanotubes

M A Zeeshan[1], K Shou[1], S Pané[1,*], E Pellicer[2], J Sort[3], K M Sivaraman[1], M D Baró[2] and B J Nelson[1].

[1]Institute of Robotics & Intelligent Systems, ETH Zürich, Switzerland

[2]Departament de Física, Facultat de Ciències, Universitat Autònoma de Barcelona, E-08193 Bellaterra, Spain

[3]Institució Catalana de Recerca i Estudis Avançats and Departament de Física, Facultat de Ciències, Universitat Autònoma de Barcelona, E-08193 Bellaterra, Spain

[*]Email: vidalp@ethz.ch

Abstract

We report on the growth and fabrication of Ni-filled multi-walled carbon nanotubes (Ni-MWNTs) with an average diameter of 115 nm and variable length of 400 nm – 1 μm. The Ni-MWNTs were grown using template-assisted electrodeposition and low pressure chemical vapor deposition (LPCVD) techniques. Anodized alumina oxide (AAO) templates were fabricated on Si using a current controlled process. This was followed by the electrodeposition of Ni nanowires (NWs) using galvanostatic pulsed current (PC) electrodeposition. Ni NWs served as the catalyst to grow Ni-MWNTs in an atmosphere of H_2/C_2H_2 at a temperature of 700^{o}C. Time dependent depositions were carried out to understand the diffusion and growth mechanism of Ni-MWNTs. Characterization was carried out using scanning electron microscopy (SEM), focused ion beam (FIB) milling, transmission electron microscopy (TEM), Raman spectroscopy and energy dispersive X-ray spectroscopy (EDX). TEM analysis revealed that the Ni nanowires possess fcc structure. To understand the effects of the electrodeposition parameters, and also the effects of the high temperatures encountered during MWNT growth on the magnetic properties of the Ni-MWNTs, vibrating sample magnetometer (VSM) measurements were performed. The template based fabrication method is repeatable, efficient, enables batch fabrication and provides good control on the dimensions of the Ni-MWNTs.

1 Introduction

Major advances in nanotechnology and drug design will enable, in the near future, the fabrication of tiny biomedical devices that are able to perform surgery and drug delivery in remote locations of the human body. The use of minimally invasive, nanometer-sized medical platforms will offer several advantages over classical medicine. Patients will benefit from fewer side effects of systemic drug administration, shorter recovery times after surgeries, and reduced post-operative pain. Additionally, such platforms would enable earlier disease diagnosis. With their large surface-area-to-volume ratio, tunable physical properties, and their ability to be functionalized with various molecules, nanostructured materials have emerged as promising candidates for drug delivery systems. Specifically, the use of magnetic nanomaterials, such as nanoparticles, nanowires (NWs) and nanodots, has been proposed because they can be guided wirelessly by using external magnetic fields [1]. Among the wide different geometries, magnetic NWs are of great advantage because they possess high magnetic moments, which in turn, favor their wireless actuation [2].

Several strategies can be used to chemically functionalize ferromagnetic NWs. The simplest approach consists of binding molecules directly on the ferromagnetic NWs surface. Tanase et al [3] show the magnetic manipulation of nickel NWs functionalized with luminescent porphyrins. To increase their functionality, NWs consisting of segments of different materials can also be synthesized. Due to the specific surface chemistry of each segment, several molecules can be selectively linked along the NW [4]. Another means of promoting the attachment of chemical species is by coating the NW body with a shell of a polymeric [5] or carbonaceous material. Carbon capsules, such as fullerenes or carbon nanotubes (CNTs), are particularly attractive for drug delivery purposes since there is a broad range of chemical methods available to exohedrally functionalize them [6-8]. Also, carbon shells serve as protective coatings on ferromagnetic NWs, minimizing their magnetic coupling and agglomeration.

Many approaches have been adopted to produce hybrid nanostructures of CNT's containing ferromagnetic nanostructures in their core. Methods of filling CNTs with nanoparticles [9] or with precursor salts that can eventually produce nanoparticles [10, 11] have been reported. These methods suffer from some drawbacks, such as low yield of filled CNTs, deposition of metallic material on the

outer surface of CNTs, and limitations imposed by capillary forces [12]. The formation and filling of CNTs can also occur simultaneously through the pyrolysis of aerosols of organometallic compounds; metallocenes can serve as a source of both the carbon shell and the magnetic core [13]. However, pyrolysis of aerosols leads to a partial and discontinuous filling of the CNTs [14]. A more convenient method of producing magnetic carbon-based shells is by the template-assisted chemical vapor deposition (CVD) [15].

Porous anodized alumina oxide (AAO) templates are widely used in fabrication of nanostructures due to the tunability of their pore dimensions [16]. AAO templates can also function as catalysts for CNT deposition [17]. Therefore, metal-filled CNTs can be grown within the template, either before or after the deposition of ferromagnetic material inside the pores. Gao et al [18] show the synthesis of CNTs by pyrolysis of polyaniline in AAO templates followed by the electrodeposition of iron, nickel and cobalt. But this approach has the drawback that the low wettability and the roughness of the inner wall of CNTs leads to a discontinuous filling [12]. To achieve continuous filling, ferromagnetic NWs can be used as catalysts around which CNTs can be synthesized. The NWs can be synthesized in AAO templates using electroless deposition [19] or electrodeposition [16]. A limited amount of previous work related to CNT formation around electrodeposited magnetic nanowires has been reported. Liu et al. show the production of Fe NWs encapsulated in shells of amorphous carbon [12]. In their work, a poor graphitization on the Fe NWs surface was observed. Recently, electrodeposited Ni NWs have been coated by graphene [20], although in this work, the AAO template is removed before the deposition of carbon. Furthermore, nickel is selectively etched away in order to study the electrical conductivity of the resultant CNT.

In this paper, a process to produce a high-yield of electrodeposited Ni NWs coated with CNTs is presented. First, a one-step anodization of aluminium (Al) evaporated on silicon is performed. Although the anodization process has been widely studied for bulk Al sheets, fabricating AAO onto silicon substrates remains a topic of research [21]. The main challenge resides in the limited thickness of the deposited Al on the silicon. There are some studies of anodized sputtered and evaporated aluminum in the literature [21, 22]. In this work, results on the anodized Al on silicon substrates with

an interlayer of gold are additionally presented. After the anodization step, electrodeposition of nickel NWs into the porous AAO template at different current densities is performed. Subsequently, CNTs are grown by low-pressure chemical vapor deposition (LPCVD) using a mixture of acetylene and hydrogen. Time and temperature studies were carried out in order to understand the growth and diffusion process of carbon nanotubes with a ferromagnetic core. Structural and magnetic characterization of the Ni NWs and the nickel-filled carbon shells are also presented.

2 Experimental Description

The process flow described in figure 1 describes the main steps required to produce high quality Ni-Multi-Walled Carbon Nanotubes (MWNTs).

2.1 E-Beam Evaporation

The substrates consisted of 10 x 10 mm silicon chips (crystal orientation (111), p-type, resistivity 0.005Ωm - 0.02Ωm, Prolog Semiconductor) with a titanium (Ti) seed layer of 6 nm, a gold (Au) layer of 12 nm, and an aluminum (Al) layer of 1.2 – 2 μm successively deposited through e-beam evaporation (Edwards E306A, Edwards, UK). A 1 μm-thick silicon dioxide insulating layer was deposited on the backside by means of plasma-enhanced chemical vapor deposition (PECVD 80+, Oxford Instruments, UK) (see figure 1a).

2.2 Anodic Alumina Oxide Templates (AAO)

AAO templates with a uniform and parallel porous structure (figure 1b) were obtained on an area of 0.5 cm^2 by one-step anodic oxidation of aluminum in a solution of 0.3 M oxalic acid ($H_2C_2O_4$, >99%, Sigma) at a constant potential of 60V. The anodization was performed in a one-compartment two-electrode cell. Distilled water from a cryostat (F-25, Julabo, Germany) was circulated in the outer jacket of the cell to maintain the working temperature at 5 °C. A lead sheet was used as the cathode. In order to minimize both concentration and thermal gradients, a constant magnetic stirring regime of 1000 rpm was combined with continuous bubbling of N_2 through the electrolyte. After anodization, the samples were rinsed with Millipore Milli-Q water. Subsequently, the specimens were kept in a 5%

phosphoric acid (H_3PO_4, >98%, Sigma-Aldrich) solution for 45 min at room temperature in order to widen the pores and decrease the thickness of the barrier layer (see figure 1c).

2.3 Electrodeposition of Ni NWs

Electrodeposition of Ni NWs inside the porous AAO template (figure 1d) was carried out in a one compartment double walled three-electrode electrochemical cell. To promote uniform filling of the pores with Ni nanowires, galvanostatic pulse current (PC) electrodeposition was performed [23, 24]. The electrolyte was a typical Nickel Watts bath containing 300 $g \cdot l^{-1}$ nickel sulfate heptahydrate ($NiSO_4 \cdot 7H_2O$, >99%, Sigma), 45 $g \cdot l^{-1}$ of nickel chloride hexahydrate ($NiCl_2 \cdot 6H_2O$, >98%, Sigma-Aldrich) and 45 $g \cdot l^{-1}$ of boric acid (H_3BO_3, >98%, Sigma) [23]. The pH was adjusted to 4.5 with a 1 M sodium hydroxide (NaOH) solution. All the depositions were carried out at a fixed temperature of 35 $^{\circ}C$ with a constant stirring rate of 200 rpm. Counter and working electrodes were connected to a programmable high performance potentiostat (Autolab PGSTAT302N, Ecochemie, The Netherlands) that was controlled by the NOVA 1.6 software. The Ni NWs were obtained by means of galvanostatic pulses at different current densities (j varied between -50 mA cm^{-2} and -150 mA cm^{-2}). Each pulse with a duration of t_{on} = 8 ms was alternated with a rest phase with a duration of t_{off} = 600 ms, having a duty cycle $t_{on}/(t_{on} + t_{off})$ of 1.3%. The t_{off} phase was incorporated to help replenish the ion concentration at the base of the pores [24]. The number of cycles for each current density was adjusted in order to keep constant the charge density at Q = 900 C cm^{-2}.

2.4 Low Pressure Chemical Vapor Deposition of CNTs

Carbon nanotubes were synthesized on the Ni NWs – AAO templates (figure 1e) using a multi-step low pressure chemical vapor deposition process (LPCVD) operating at a base pressure of 10^{-5} mbar (PEO 603 PLC-300C, ATV Technologie GmbH, Germany). AAO templates filled with Ni NWs were rinsed thoroughly with deionized water, dried with N_2 gas and were placed inside the quartz tube of the LPCVD chamber. The LPCVD system can be operated at a base pressure of 10^{-5} mbar [25]. The chamber temperature was ramped at a rate of 41 °C per minute to the desired temperature (600 – 700 °C) and was allowed to stabilize for 3 minutes. After venting the chamber, H_2 gas was pumped into the chamber at a rate of 3 standard liters per minute (slm). The gas was switched off after 31 s to maintain

the pressure at 300 mbar. Since a native oxide is formed on the exposed surface of Ni NWs, a subsequent reducing H_2 environment was maintained for 12 min in order to reduce the oxide layer and to activate the surface of Ni NWs. H_2 was partially removed from the furnace and a mixture of H_2 and 10% C_2H_2 in He were introduced into the chamber. H_2 was pumped in for 37 s at a rate of 1 slm and C_2H_2 for 42 s at a rate of 0.5 slm. The final ratio of the H_2:C_2H_2 mixture was 20:1 with a total chamber pressure of 200 ± 5 mbar. Carbon was deposited around the Ni NWs by varying the deposition time from 15 min to 60 min. As C_2H_2 is a highly concentrated gas source and decomposes at a lower temperature, side products, such as amorphous C, are generated during the growth process. Therefore, all the gasses were pumped out to remove residual gasses. Etching with H_2 gas was performed so that unwanted carbon on the CNTs could be transformed into hydrocarbon (C_mH_n) gasses. H_2 was pumped in for 20 s at a rate of 3 slm to obtain a total pressure of 300 mbar. Etching was performed for 1 hour. The chamber was cooled to 40 °C in a N_2 environment.

2.5 Characterization

AAO templates were dissolved in 10 wt% NaOH at a temperature of 90 ºC. This left an array of Ni nanowires coated with CNTs which was washed thoroughly using ethanol. The morphology of AAO templates, Ni NWs and Ni-filled carbon nanostructures was observed in a scanning electron microscope (SEM, Zeiss NVision 40, Carl Zeiss, Germany) equipped with a focused ion beam (FIB). FIB milling was used to observe the cross section of AAO templates before and after the deposition of nanowires. The chemical composition of the composite nanostructures was analyzed by means of energy dispersive X-ray spectroscopy (EDAX Inc., USA). Transmission electron microscopy (TEM) was used to observe the shell structure of the CNTs (Cm12, operated at 100 kV, Philips, Netherlands) and to perform selected area electron diffraction (SAED) analysis (Jem 2011, operating at 200 kV, Jeol, Japan). Ni-MWNTs were dispersed ultrasonically in ethanol and were placed onto Cu-grid with holey carbon for carrying out TEM characterization. Raman spectra were recorded at room temperature from a WITec CRM200 confocal-Raman spectroscope using a 532 nm green laser. The spectrometer is mounted with a Peltier-cooled charge coupled device (CCD) camera. The relative spectral resolution was 1 cm^{-1}. The magnetic properties of the Ni NWs embedded in the AAO

templates were evaluated at room temperature using a vibrating sample magnetometer (VSM) from Oxford Instruments. Hysteresis loops were recorded both along and perpendicular to the NWs axis. From the loops, the squareness ratio and coercivity values were determined for the different current densities used in the electrodeposition of the NWs. In addition, the hysteresis loops of CNTs filled with Ni NWs, grown at the current density of -100 mA cm^{-2}, were measured as a function of the carbon coating time.

3 Results and Discussion

3.1 AAO templates

AAO templates with uniform and parallel porous structure are obtained by anodic oxidation of aluminum in solution of 0.3 M oxalic acid at a constant potential. Figure 2 shows the current density *j* response plotted as a function of time at 60 V. Initially, the exponential drop in *j* from very high values is due to the growth of a homogenous planar oxide [26]. The initial minimum in the curve (figure 2, section A) and its stabilization (figure 2, section B) are related to the nucleation of the pores and the creation of the porous layer, respectively. The time required to achieve a stable porous AAO template in oxalic acid electrolytes has been reported to be 15-20 min [26]. In this work, the time required to achieve the stabilization of current is only around 30 s, probably due to the fact that the anodization was performed on relatively thin aluminium. The slight decrease in *j* observed just after 4 min (figure 2, section C) corresponds to a decrease in resistivity due to depletion of Al in the interface substrate / electrolyte, and the further increase indicates the occurrence of oxygen evolution, because the electrolyte has reached the gold layer [21].

Figure 3a represents a typical top-view SEM image of as-anodized aluminum layer. Pores exhibited a diameter (P_D) of 25-30 nm and, as expected from a one-step anodization process, were randomly distributed [24]. A subsequent chemical pore widening treatment consisted of immersing the template in 5% H_3PO_4 for 45 minutes at room temperature and increased P_D to 90-105 nm at an approximate rate of 2 $nm.min^{-1}$ (figure 3b). Interpore distance (I_{PD}) varied between 117-145 nm. The remaining barrier layer was roughly 20-30 nm thick. Therefore, no additional barrier layer-thinning procedure was applied since the use of subsequent high current density during electrodeposition supersedes the

limitations [23, 24]. Pore density is around $5x10^9$ on an area of 0.5 cm^2. Figure 3c shows a cross section view of the AAO templates with cylindrical pores having a depth of around 900nm.

3.2 Pulsed-current electrodeposition of Ni NWs

Pulsed-current electrodeposition was performed at different current densities in order to study its influence on the structure and magnetic properties of the Ni NWs. Figure 4 shows the potential response when applying current density pulses of -100 mA cm^{-2} for 8 ms. After each pulse, a rest phase (no current) was applied for 600 ms in order to replenish the electrolyte inside the pores. One can observe that the values of potential corresponding to each pulse were higher at the first cycles and lower for the last ones. This is related to the initial nucleation of nickel at the base of the pores. During the rest phase, a capacitive discharge is observed [23, 26]. FIB cross-sections were taken in order to estimate the NWs length and the degree of filling (figure 5a and 5b). For all conditions, uniform filling of the AAO templates was observed. The average length of the NWs increased with the galvanostatic pulse from 450 nm at -50 mA cm^{-2} to 680 nm at -100 mA cm^{-2} and 900 nm at -125 mA cm^{-2}, and decreased further on (500 nm at -150 mA cm^{-2}). This result can be explained, at least in part, on the basis of the dependence of cathodic current efficiency with current density on porous substrates [27]. Figures 5c and 5d show TEM images of Ni NWs electrodeposited at pulses of -125 mA cm^{-2} and -150 mA cm^{-2}, respectively. Enhanced hydrogen co-evolution at -150 mA cm^{-2} could be the reason for the growth of shorter Ni NWs with respect to the scenario at -125 mA cm^{-2}. In agreement with FIB observations, the diameter of the NWs is around 115 nm. However, this value is about 10% higher than the P_D of the parent template. This is probably due to the mechanical strain exerted on the AAO pores by the growing Ni NWs. The inset of figure 5c shows the corresponding SAED pattern. As expected, the NWs are highly crystalline. The indexed spots match with the face-centered cubic (fcc) phase of Ni.

3.3 Effect of growth parameters on Ni – MWNTs

A series of experiments were carried out to optimize growth parameters for the CNTs. Time and temperature dependency were investigated. Since temperature determines the decomposition rate of the precursor and the crystalline structure of the resulting CNTs, the effect of temperature in the range

of 600°C to 700°C was studied. It was observed that the catalytic growth of nanotubes started at 600 °C, but few nanotubes were observed at this temperature. A higher density of tubes was obtained at 650 °C. The optimal coverage of the NWs with CNTs was achieved at 700 °C. At this temperature, different deposition times (15 – 60 min) were applied. It was found that the growth of CNTs started during the first 15 min; probably the precursor gas required a longer time to diffuse through a large catalyst. A uniform carbon coating could be found around the NWs for times of 30 min and more. There were no significant improvements with longer deposition times, though from TEM analysis a slight difference in interlayer spacing was found. Interlayer spacing of Ni-MWNT was reduced from 0.414 nm (30 min) to 0.354 nm (1 hr) whereas interlayer spacing at 45 min depositions was found to be 0.384 nm. Figure 6a shows an SEM image of a vertical array of Ni-filled CNTs after the removal of AAO template. Ni NWs are fully encapsulated inside carbon shells. Small CNTs were also found on the surface of Ni-filled CNTs, which could be formed due to the catalytic action of residual nickel oxides and hydroxides from the electrodeposition bath. Figure 6b shows an EDX spectrum of Ni-filled CNTs. EDX spectrum also confirms the filling of Ni nanowires by carbon. In most cases, nanotube filling was continuous and the diameter did not significantly vary. TEM observations showed that NWs were coated by a combination of amorphous and graphitized sp^2 carbon. A TEM image of a Ni NW encapsulated by a MWNT is displayed in figure 7a. The magnifications in figures 7b and 7c show graphitized carbon on both sides of the NW. The thickness of the shells on the right and on the left of the NW was 17.5 nm with an interlayer spacing of 0.345 nm, which corresponds to 50 shells. Amorphous carbon was also observed as shown in figure 7d. In some cases, Ni-filled MWNTs were found to have a sharp tip (figure 8). This extrusion phenomenon can be related to a compressive stress caused by the CNTs on the NWs surface, which occurs at high temperature. Sun et al [28] studied the extrusion effect in carbon nanotubes encapsulating iron, iron carbide and cobalt NWs by irradiating the nanostructures with an electron beam at 600 °C. The collapse of the carbon structure started in the empty portion of the capsule and aggregated at the NW cap. When the irradiation was maintained, the narrow part of the NW was eventually severed. A similar process that occurs during the growth of the carbon shells may be the reason behind the tip thinning seen in this work. The stress exerted by the growth of successive layers of carbon can shrink the tip of the Ni NW. Figure 8c shows a NW with an

extruded tip. The tip diameter was 24 ± 5 nm and the carbon shell diameter all along the extruded tip is around 41 nm.

Complementary Raman analyses were carried out to characterize the structure of the carbon coating. Figure 9 shows the Raman spectrum of Ni-MWNTs obtained at a laser excitation wavelength of 532 nm. Two main peaks can be observed in the first-order spectrum. The peaks at a Raman shift of 1342 cm^{-1} (D band) and 1582 cm^{-1} (G band) are typical of MWNTs. The former is the so-called defect-induced D band, whereas the latter is related to vibrations in all sp^2 carbon materials [29]. The intensity ratio of the D band to the G band is $I_D/I_G = 0.84$, indicating a significant graphitization degree of the capsules.

3.4. Magnetic properties

Magnetic measurements were performed at room temperature on the Ni NWs embedded in the AAO templates. Typical hysteresis loops corresponding to the arrays of Ni NWs grown at j = -50 and -100 mA cm^{-2}, measured both along and perpendicular to the NW axis, are shown in figures 10a and 10b. The Ni NWs exhibit coercivity values, H_C, ranging from 200 to 450 Oe when the magnetic field is applied along the NW axis and around 100-150 Oe when the field is perpendicular to the NW axis (see figure 10d). The tilted shape of the loops and the relatively low H_C and the ratio between the remanent and saturation magnetization, M_R/M_S, values are in agreement with the results reported in the literature for polycrystalline Ni NWs with relatively large diameter and low aspect ratios, which show incoherent magnetization reversal [30-32]. The shape of the hysteresis loops and, in particular, M_R/M_S, slightly varies depending on the direction of measurement (see figure 10e), an effect which can be attributed to the magnetic shape anisotropy of the NWs. Dipolar inter-wire interactions can also have an influence on the overall shape of the loops, reducing both H_C and M_R/M_S [33]. The dependence of H_C in the parallel direction (i.e. along the NW axis) as a function of the current density is linked to variations in their length. Namely, H_C increases with the length of the NWs. The highest H_C corresponds to the NWs electrodeposited at j = -125 mA cm^{-2} (i.e., the longest ones). Such an increase in the coercive field with the length of the NWs in arrayed systems has been observed both theoretically and experimentally [33].

After coating the Ni NWs with MWNTs, no significant changes were observed in the shape ogf the hysteresis loops (cf. figures 10b and 10c). The coercivity measured along the NW axis remains around 450 Oe, even after 60 min of carbon deposition (figure 10f). This suggests that the process of coating the NWs with carbon does not significantly modify their microstructure. Typically, in very long NWs, the M_R/M_S values are large which could lead to aggregation of the NWs in a fluid medium in the absence of an external magnetic field. The magnetic properties of the Ni-MWNTs obtained in this work are promising for wireless manipulation through bodily fluids.

4 Conclusions

Ni-filled MWNT have been successfully synthesized by template assisted LPCVD. By optimizing the conditions of evaporated aluminium anodization and of CNT LPCVD, magnetic hybrid nanostructures are obtained. SEM, TEM, EDX, SAED, Raman and VSM were used to characterize the Ni NWs and the Ni-MWNTs. No significant differences in terms of crystalline structure and magnetic properties were observed between the Ni NWs and the Ni-MWNTs. Therefore, this fabrication method preserves the magnetic properties of the Ni NW core. The uniformly coated Ni NWs possess a significant amount of graphitized carbon.

5 Acknowledgment

We thank the FIRST lab and EMEZ of ETH Zürich for technical support. Funding for this research was conducted from the project “Nano-Actuators and Nano-Sensors for Medical Applications (NANOMA)” funded by the European Commission under the seventh Framework Program (FP7). SP acknowledges a postdoctoral fellowship of the Spanish MICINN. EP is indebted with the Generalitat de Catalunya for the *Beatriu de Pinós* fellowship. MDB acknowledges partial financial support from an ICREA-Academia award.

References

[1] Zhang L, Petit T, Lu Y, Kratochvil B E, Peyer K E, Pei R, Lou J and Nelson B J 2010 Controlled propulsion and cargo transport of rotating nickel nanowires near a patterned solid surface *ACS Nano* **4** 6228-34.

[2] Vijay K V, Linfeng C and Jining X 2008 *Nanomedicine: design and applications of magnetic nanomaterials, nanosensors and nanosystems* (Chichester, UK: John Wiley & Sons, Ltd) pp 11-15.

[3] Tanase M, Bauer L A, Hultgren A, Silevitch D M, Sun L, Reich D H, Searson P C and Meyer G J 2001 Magnetic alignment of fluorescent nanowires *Nano Lett.* **1** 155-8.

[4] Wang J 2009 Biomolecule-functionalized nanowires: from nanosensors to nanocarriers *ChemPhysChem* **10** 1748-55.

[5] Magnin D, Callegari V, Matefi-Tempfli S, Matefi-Tempfli M, Glinel K, Jonas A M and Demoustier-Champagne S 2008 Functionalization of magnetic nanowires by charged biopolymers *Biomacromolecules* **9** 2517-22.

[6] Balasubramanian K and Burghard M 2005 Chemically functionalized carbon nanotubes *Small* **1** 180-92.

[7] Klumpp C, Kostarelos K, Prato M and Bianco A 2006 Functionalized carbon nanotubes as emerging nanovectors for the delivery of therapeutics *Biochim. Biophys. Acta - Biomembr.* **1758** 404-12.

[8] Touhara H and Okino F 2000 Property control of carbon materials by fluorination *Carbon* **38** 241-67.

[9] Jain D and Wilhelm R 2007 An easy way to produce alpha-iron filled multiwalled carbon nanotubes *Carbon* **45** 602-6.

[10] Wu H Q, Wei X W, Shao M W, Gu J S and Qu M Z 2002 Preparation of Fe-Ni alloy nanoparticles inside carbon nanotubes via wet chemistry *J. Mater. Chem.* **12** 1919-21.

[11] Capobianchi A, Foglia S, Palange E, Arrizza L, Veroli C, Mansilla M V and Fiorani D 2009 Nanocomposite Materials, *Solid State Phenom.* **151** 166-70.

[12] Liu L F, Mu S C, Xie S S, Zhou W Y, Song L, Liu D F, Luo S D, Xiang Y J, Zhang Z X, Zhao X W, Ma W J, Shen J, Wang C Y and Wang G 2006 Template synthesis, characterization and magnetic property of Fe nanowires-filled amorphous carbon nanotubes array *J. Phys. D - Appl. Phys.* **39** 3939-44.

[13] Lv R T, Kang F Y, Zhu D, Zhu Y Q, Gui X C, Wei J Q, Gu J L, Li D J, Wang K L and Wu D H 2009 Enhanced field emission of open-ended, thin-walled carbon nanotubes filled with ferromagnetic nanowires *Carbon* **47** 2709-15.

[14] Lv R T, Cao A Y, Kang F Y, Wang W X, Wei J Q, Gu J L, Wang K L and Wu D H 2007 Single-crystalline permalloy nanowires in carbon nanotubes: Enhanced encapsulation and magnetization *J. Phys. Chem. C* **111** 11475-9.

[15] Jeong S H, Lee O J, Lee K H, Oh S H and Park C G 2002 Preparation of aligned carbon nanotubes with prescribed dimensions: Template synthesis and sonication cutting approach *Chem. Mat.* **14** 1859-62.

[16] Montero-Moreno J M, Belenguer M, Sarret M and Mueller C M 2009 Production of alumina templates suitable for electrodeposition of nanostructures using stepped techniques *Electrochim. Acta* **54** 2529-35.

[17] Rummeli M H, Schaffel F, Bachmatiuk A, Adebimpe D, Trotter G, Borrnert F, Scott A, Coric E, Sparing M, Rellinghaus B, McCormick P G, Cuniberti G, Knupfer M, Schultz L and Buchner B 2010 Investigating the outskirts of Fe and Co catalyst particles in alumina-supported catalytic CVD carbon nanotube growth *ACS Nano* **4** 1146-52.

[18] Gao C L, Tao F F, Lin W W, Xu Z and Xue D 2008 Ordered arrays of magnetic metal nanotubes and nanowires encapsulated with carbon tubes *J. Nanosci. Nanotechnol.* **8** 4494-9.

[19] Zhang Z T, Dai S, Blom D A and Shen J 2002 Synthesis of ordered metallic nanowires inside ordered mesoporous materials through electroless deposition *Chem. Mat.* **14** 965-8.

[20] Wang R, Hao Y F, Wang Z Q, Gong H and Thong J T L 2010 Large-diameter graphene nanotubes synthesized using Ni nanowire templates *Nano Lett.* **10** 4844-50.

[21] Hill J J, Haller K and Ziegler K J 2011 Direct Fabrication of high-aspect ratio anodic aluminum oxide with continuous pores on conductive glass *J. Electrochem. Soc.* **158** E1-7.

[22] Kim J, Khanal S, Islam M, Khatri A and Choi D 2008 Electrochemical characterization of vertical arrays of tin nanowires grown on silicon substrates as anode materials for lithium rechargeable microbatteries *Electrochem. Commun.* **10** 1688-90.

[23] Nielsch K, Muller F, Li A P and Gosele U 2000 Uniform nickel deposition into ordered alumina pores by pulsed electrodeposition *Adv. Mater.* **12** 582-6.

[24] Sklar G P, Paramguru K, Misra M and LaCombe J C 2005 Pulsed electrodeposition into AAO templates for CVD growth of carbon nanotube arrays *Nanotechnology* **16** 1265-71

[25] Jungen A, Stampfer C, Durrer L, Helbling T and Hierold C 2007 Amorphous carbon contamination monitoring and process optimization for single-walled carbon nanotube integration *Nanotechnology* **18** 1-6.

[26] Nielsch K 2002 Hochgeordnete Ferromagnetische Nano-Stabensembles Thesis Max-Planck-Institut für Mikrostrukturphysik, Germany

[27] Napolskii K S, Roslyakov I V, Eliseev A A, Petukhov D I, Lukashin A V, Chen S-F, Liu C-P and Tsirlina G A 2011 Tuning the microstructure and functional properties of metal nanowire arrays via deposition potential *Electrochim. Acta* **56** 2378-84.

[28] Sun L, Banhart F, Krasheninnikov A V, Rodriguez-Manzo J A, Terrones M and Ajayan P M 2006 Carbon nanotubes as high-pressure cylinders and nanoextruders *Science* **312** 1191-202.

[29] González-Guerrero A B, Mendoza E, Pellicer E, Alsina F, Fernández-Sánchez C, Lechuga L M 2008 Discriminating the carboxylic groups from the total acidic sites in oxidized multi-wall carbon nanotubes by means of acid–base titration *Chem. Phys. Lett.* **462** 256-9.

[30] Nielsch K, Wehrsphon R B, Barthel J, Kirschner J, Gösele U, Fischer S F, Kronmüller H 2001 Hexagonally ordered 100 nm period nickel nanowire arrays *Appl. Phys. Lett*. **79** 1360-2.

[31] Sellmyer DJ, Zheng M, Skomski R 2001 Magnetism of Fe, Co and Ni nanowires in self-assembled arrays *J. Phys.: Condens. Matter.* **13** R433-60.

[32] Qin J, Nogués J, Mikhaylova M, Roig A, Muñoz J S and Muhammed M 2005 Differences in the Magnetic Properties of Co, Fe, and Ni 250-300 nm Wide nanowires electrodeposited in amorphous anodized alumina templates *Chem Mater* **17** 1829-34.

[33] Escrig J, Lavín R, Palma J L, Denardin J C, Altbir D, Cortés A and Gómez H 2008 Geometry dependence of coercivity in Ni nanowire arrays *Nanotechnology* **19** 075713.

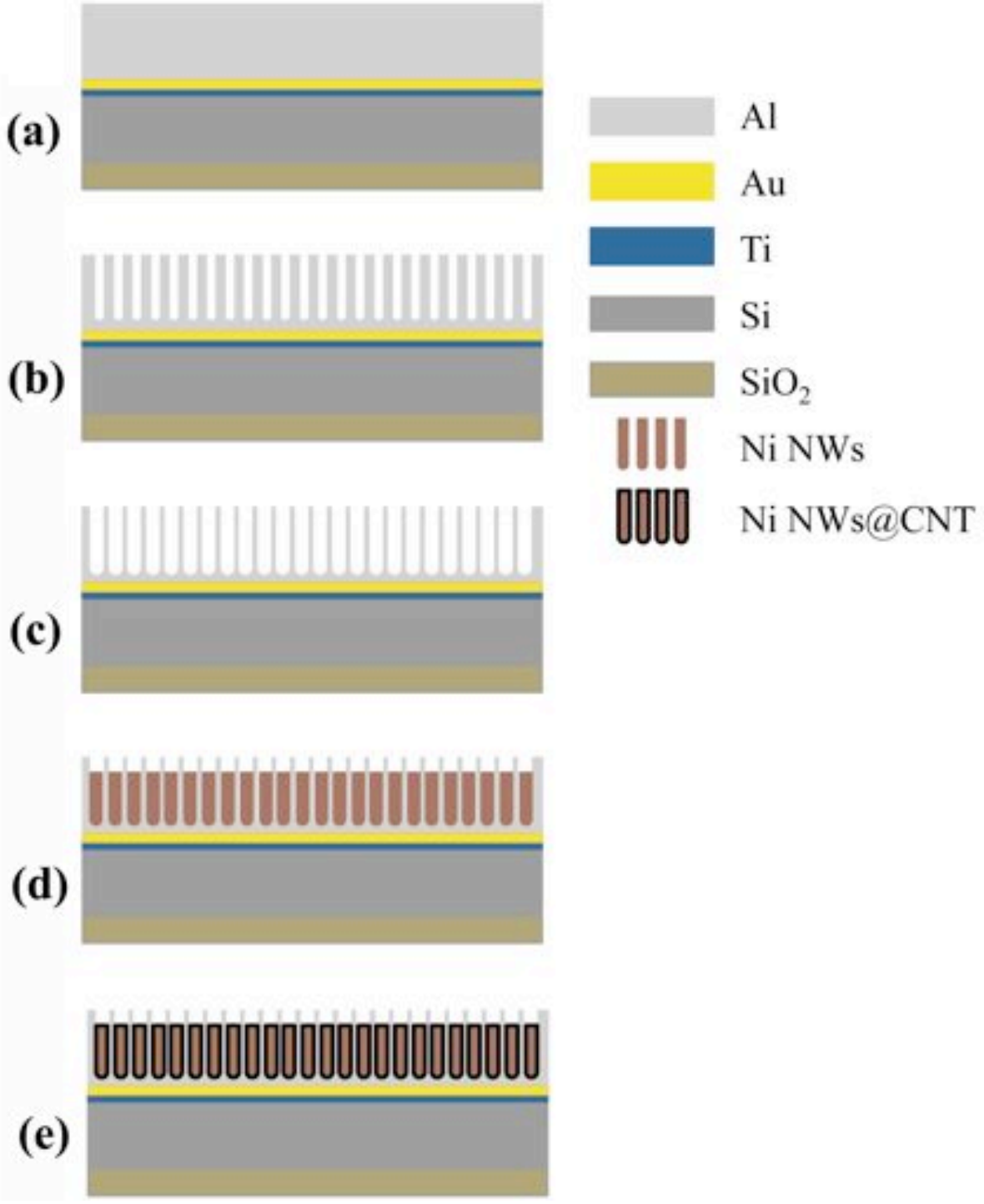

Figure 1. Schematic of the synthesis process of Ni filled CNTs (a) Multi-layer metal evaporation onto silicon substrate. (b) AAO template after anodization in oxalic acid. (c) Pore widening and barrier layer thinning. (d) Galvanostatic pulse current (PC) electrodeposition of Ni NWs inside AAO (e) Ni-Filled CNTs grown under LPCVD at 700 $^{\circ}$C.

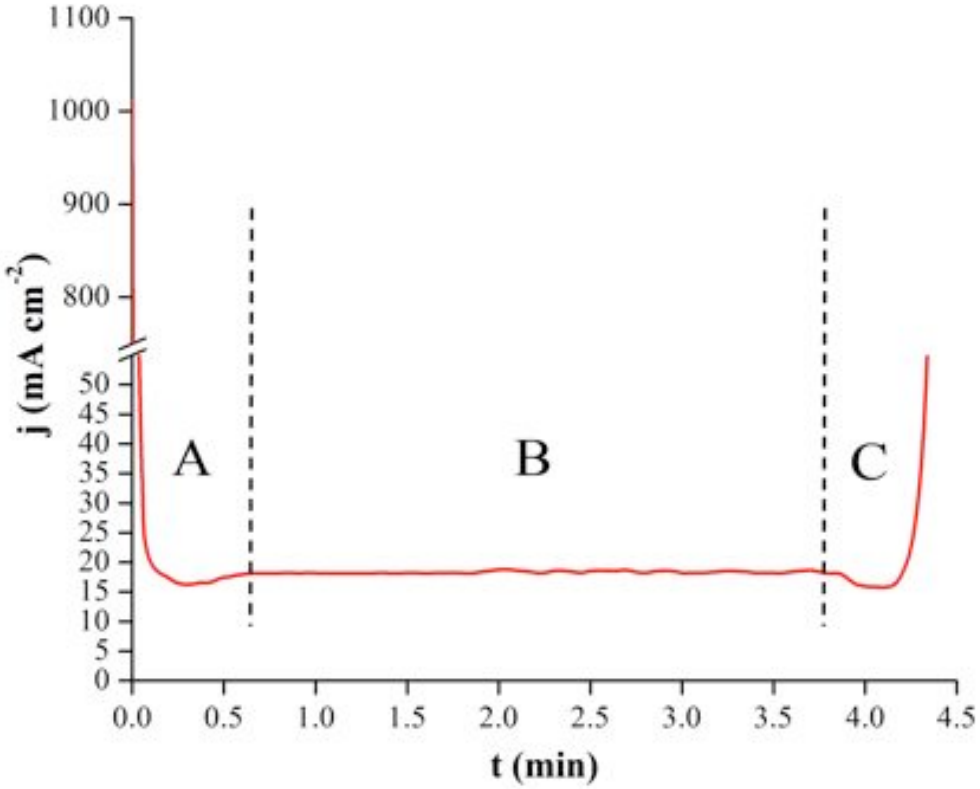

Figure 2. Potentiostatic curve showing the anodization process of evaporated aluminum on silicon chips at 60 V and 5 °C under stirring conditions.

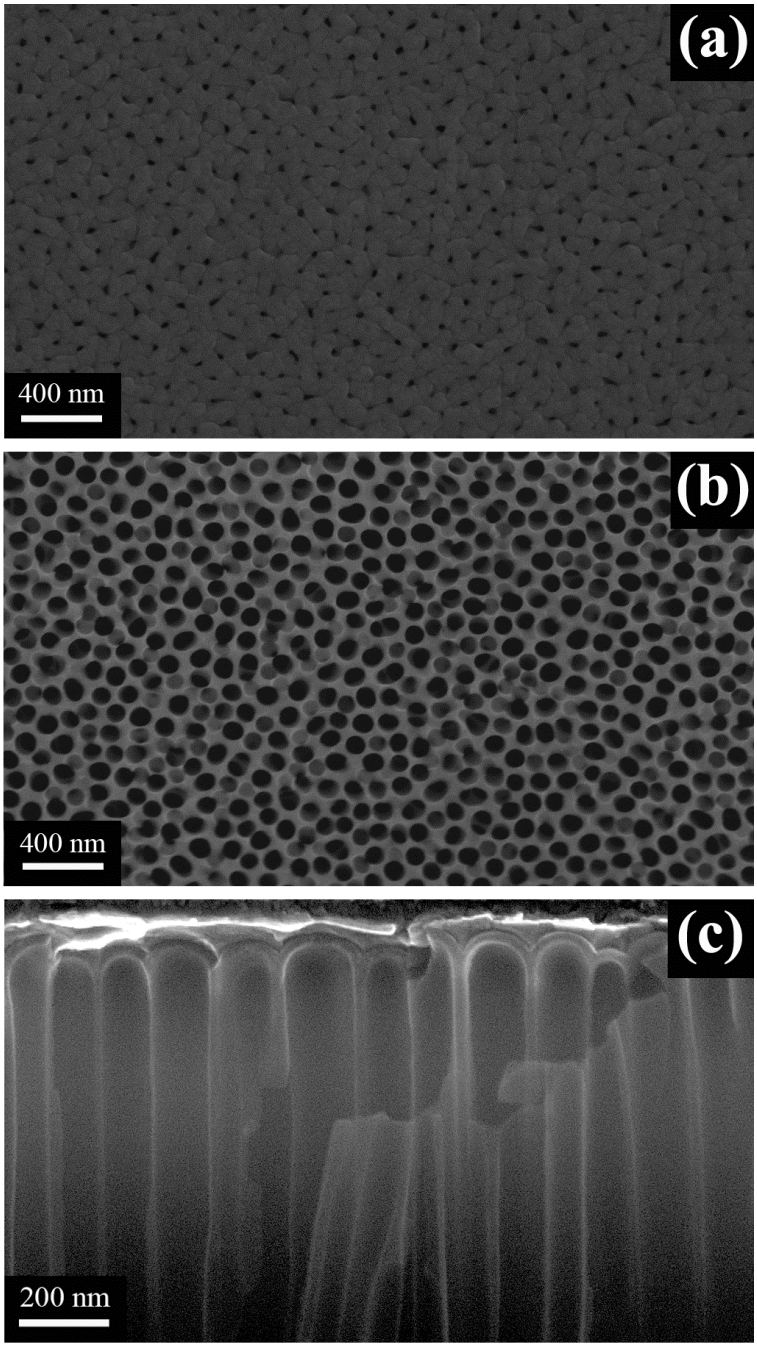

Figure 3. SEM images of (a) AAO templates without pore widening have a pore diameter (P_D) of approximately 30nm. (b) AAO templates after treatment in 5 wt% H_3PO_4 at room temperature. P_D is 100nm (c) A cross sectional view of AAO templates

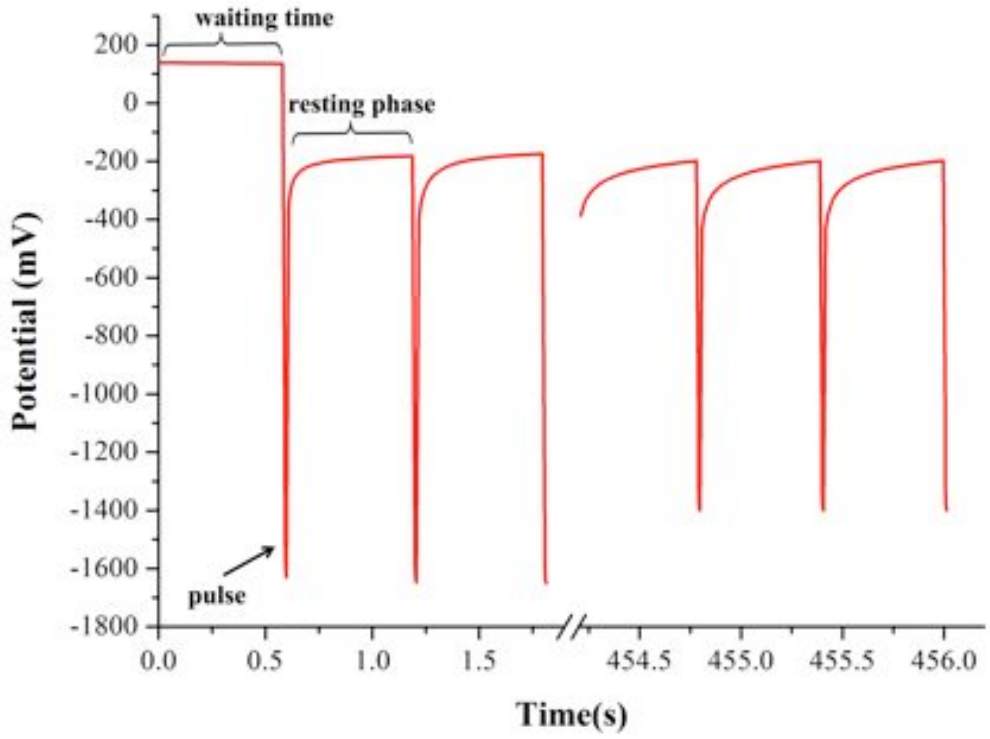

Figure 4. Potential response versus time with a fixed pulse current density of -100mA cm-2. After the pulse, a potential stabilization towards -200 mV is observed during the resting phase and corresponds to a capacitance discharge.

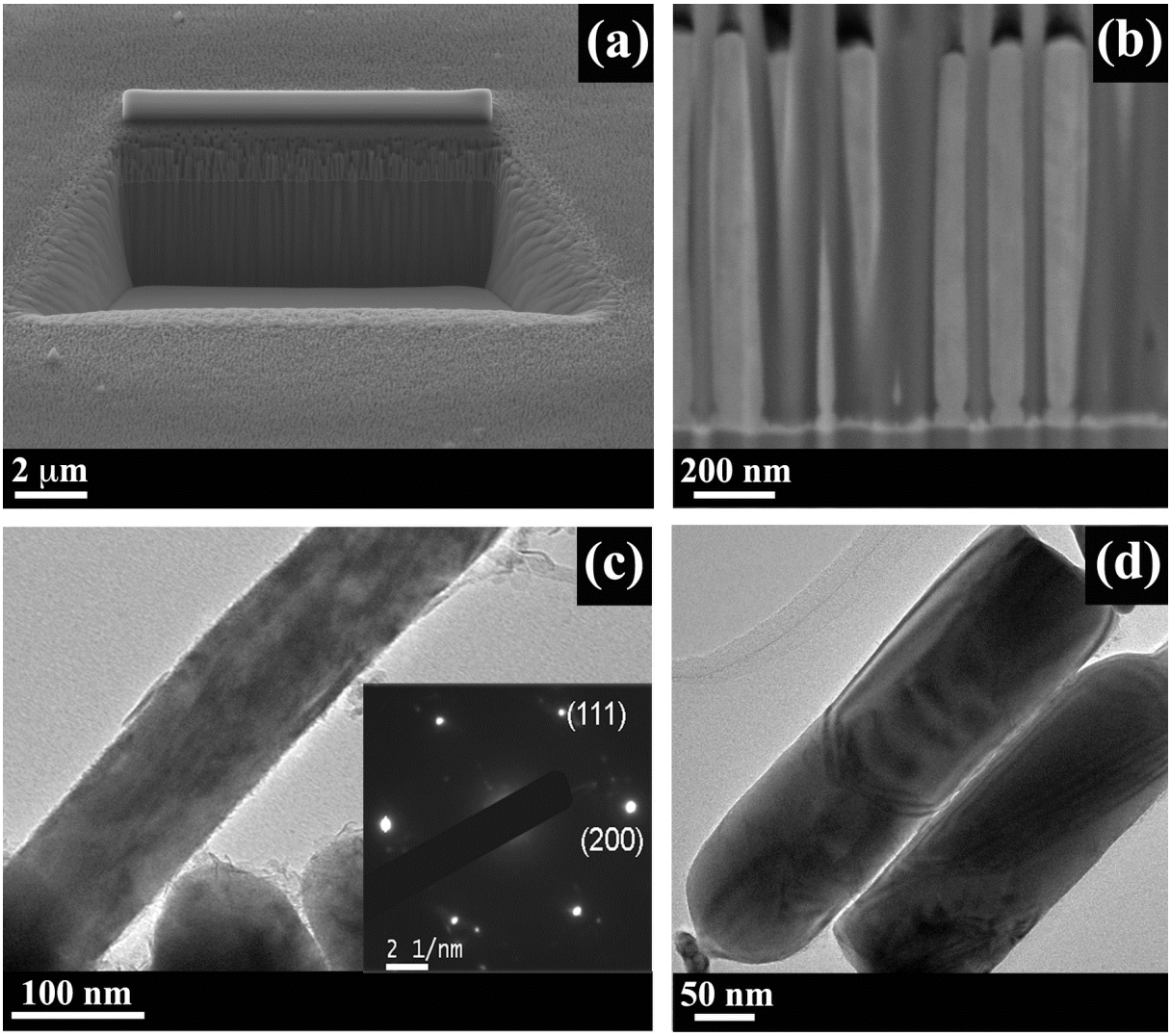

Figure 5. (a) SEM of a cross-sectional view of an AAO template filled with electrodeposited Ni NWs at -125 mA cm-2. The cross-section was obtained by FIB milling. (b) SEM magnification of a FIB cross-section showing a uniform filling of pores. (c) TEM picture of Ni NWs obtained at galvanostatic pulses of -125 mA cm-2. The inset shows a SAED pattern, which indicates the fcc crystalline structure of the NWs. (d) TEM picture of NWs obtained at galvanostatic pulses of -150 mA cm-2.

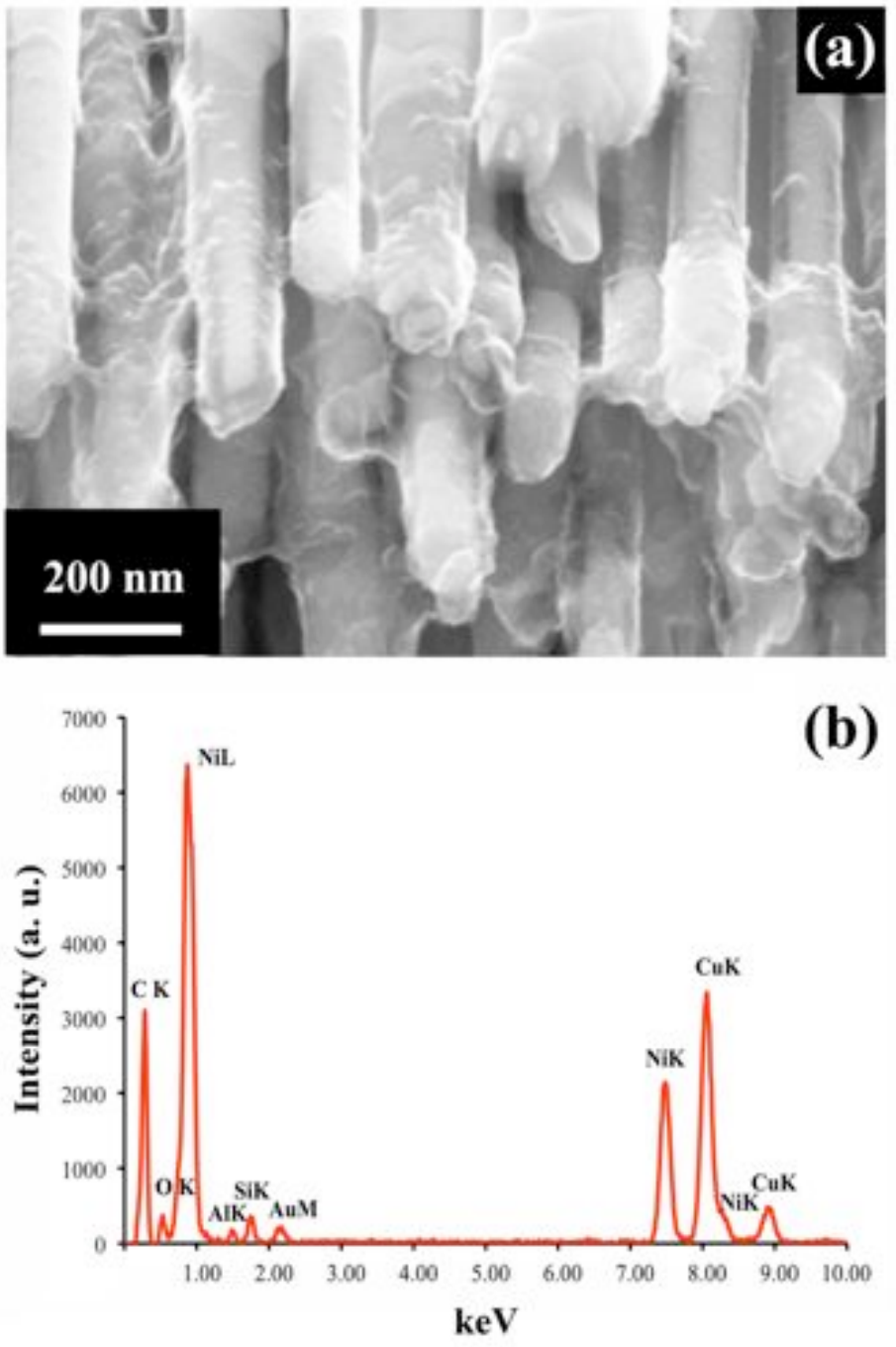

Figure 6. (a) SEM image of an array of Ni-MWNTs after removal of the AAO templates. (b) EDX spectra obtained by spotting on the composite nanostructure during a TEM observation. The peak corresponding to Cu is due to the TEM grid.

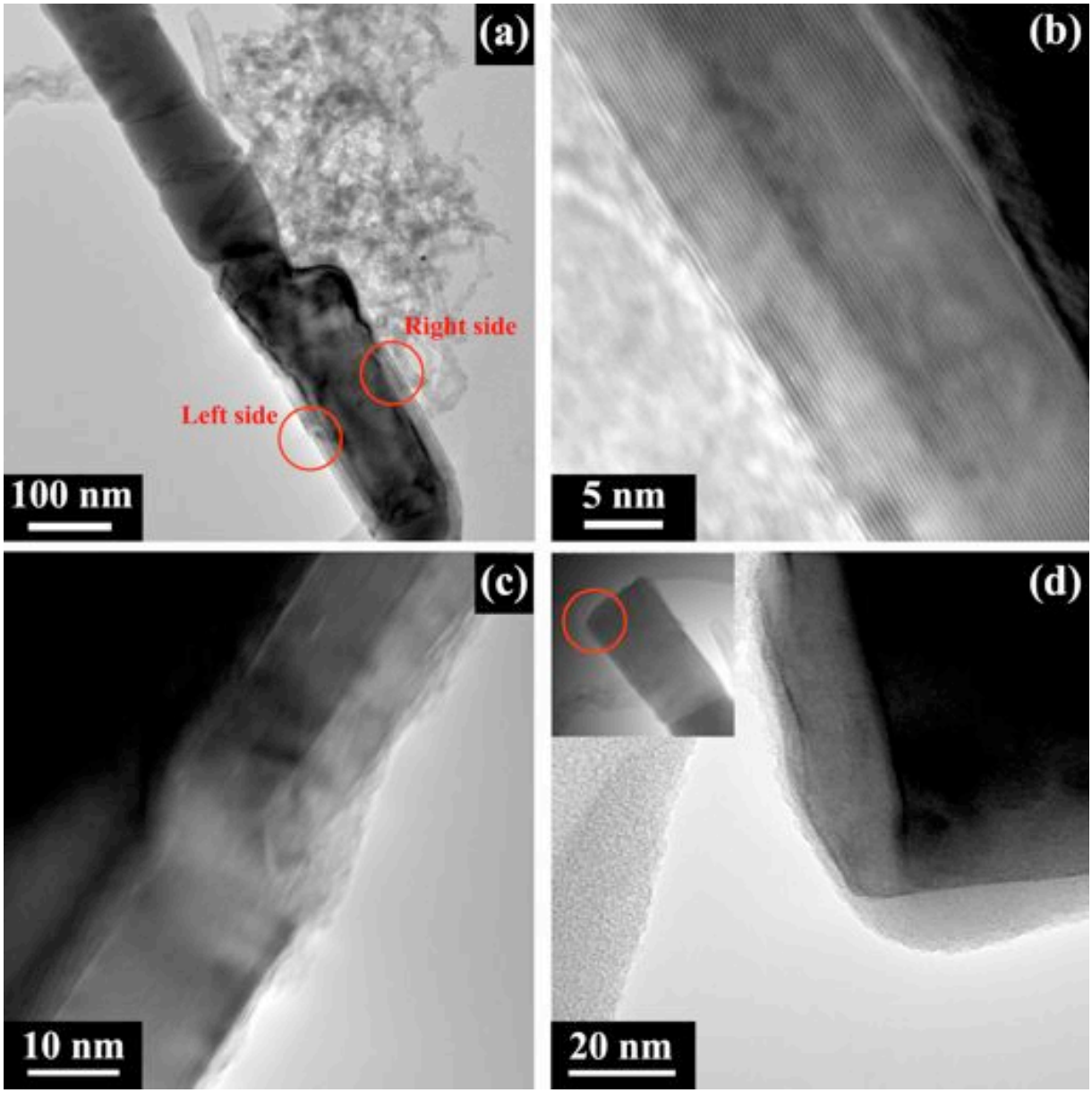

Figure 7. (a) TEM picture of a Ni-MWNT. (b), (c) and (d) Magnifications of the right side, the left side and the tip of a Ni-MWNT showing the interface of the Ni NW and the C capsule. In the regions shown in magnifications (b) and (c), carbon shells with sp2 hybridization are displayed, whereas amorphous carbon is observed in (d). Despite being uniformly coated, the Ni NWs are coated by a mixture of amorphous and sp2 carbon. Inset in (d) shows a lower magnification view of the tip.

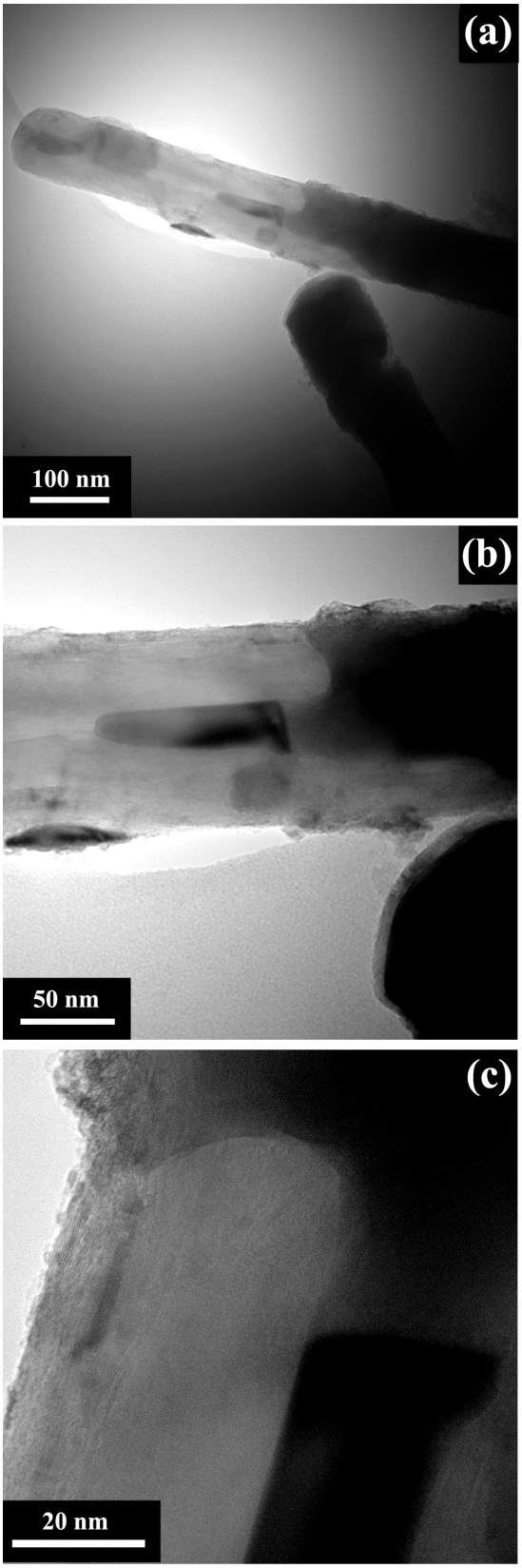

Figure 8. (a) TEM image showing a Ni-MWNT with an extruded tip. (b) Magnification of the tip. (c) Magnification showing the interface tip and carbon coating. In this case, sp^2 carbon is observed in this region.

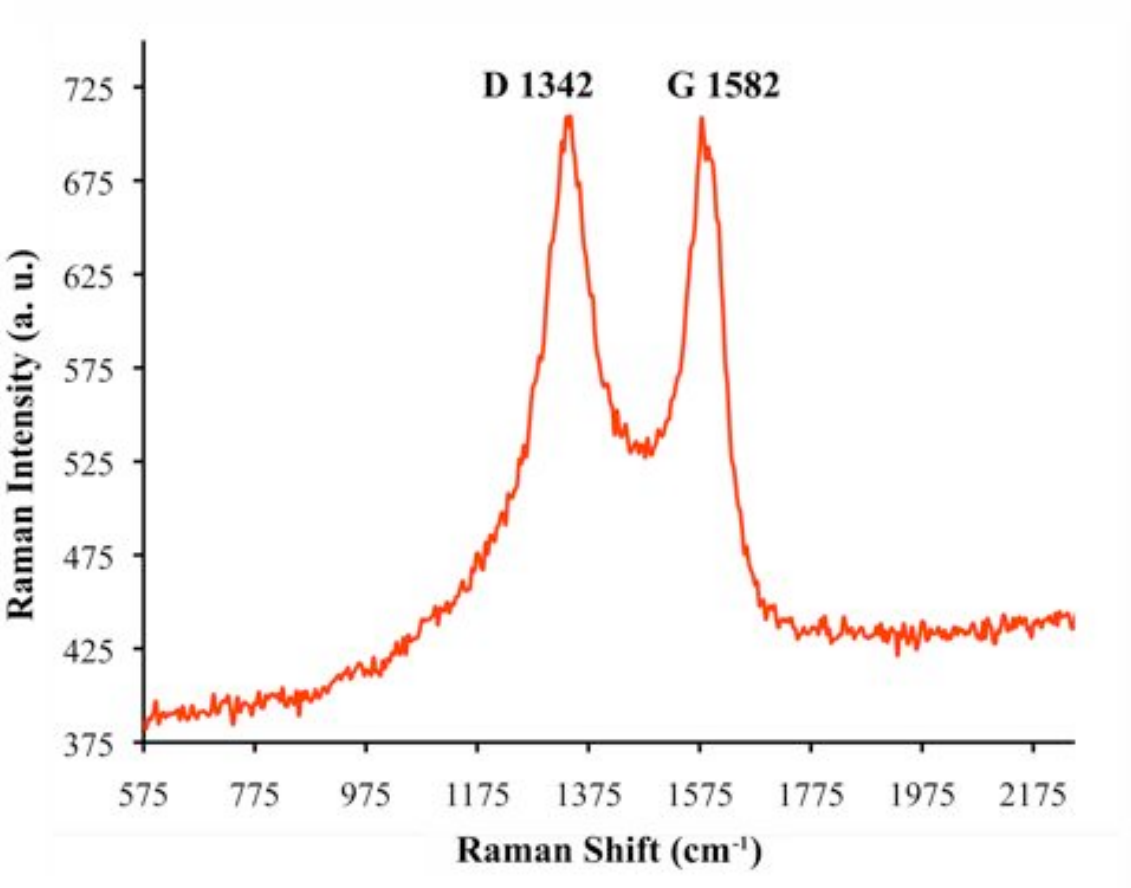

Figure 9. Room temperature Raman spectrum of Ni-MWNTs taken with 532 nm laser wavelength. The spectrum shows a typical MWNT pattern with D- and G- bands.

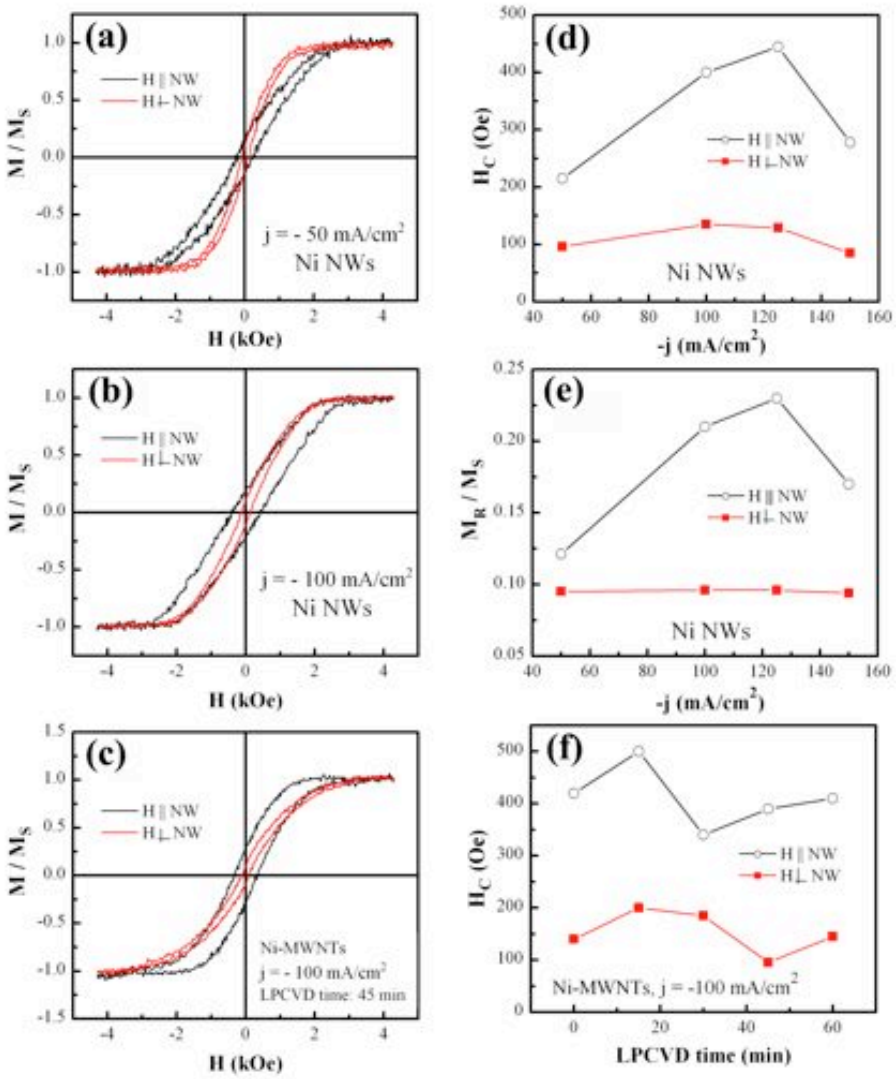

Figure 10. (a) Normalized hysteresis loops corresponding to the uncoated Ni NWs grown at a galvanostatic pulse of j = -50 mA cm-2 embedded inside the pores of the AAO template, measured along and perpendicular to the nanowire axis. (b) normalized hysteresis loops corresponding to the uncoated Ni NWs grown at j = -100 mA cm-2 embedded inside the pores of the AAO template, measured along and perpendicular to the nanowire axis. (c) normalized hysteresis loops corresponding to the Ni NWs grown at j = -100 mA cm-2 and subsequently carbon coated using a LPCVD time of 45 min, measured along and perpendicular to the nanowire axis. (d) dependence of the coercivity, H_C, as a function of the current density, j, for the uncoated Ni NWs measured along and perpendicular to the NW axis. (e) dependence of the squareness ratio, MR/MS, as a function of the current density, j, for the uncoated Ni NWs measured along and perpendicular to the NW axis. (f) dependence of HC on the LPCVD time, both along and perpendicular to the NW axis direction, for Ni-MWNTs (the NiWs were electrodeposited at j = -100 mA cm-2).